



**HAL**  
open science

## **Lamb wave attenuation in a rough plate. I. Analytical and experimental results in an anisotropic plate**

Catherine Potel, Damien Leduc, Bruno Morvan, Claude L. Depollier, Anne-Christine Hladky, Jean-Louis Izbicki, Philippe Pareige, Michel Bruneau

► **To cite this version:**

Catherine Potel, Damien Leduc, Bruno Morvan, Claude L. Depollier, Anne-Christine Hladky, et al.. Lamb wave attenuation in a rough plate. I. Analytical and experimental results in an anisotropic plate. *Journal of Applied Physics*, 2008, 104 (7), pp.074908. 10.1063/1.2979850 . hal-00360340

**HAL Id: hal-00360340**

**<https://hal.science/hal-00360340>**

Submitted on 25 May 2022

**HAL** is a multi-disciplinary open access archive for the deposit and dissemination of scientific research documents, whether they are published or not. The documents may come from teaching and research institutions in France or abroad, or from public or private research centers.

L'archive ouverte pluridisciplinaire **HAL**, est destinée au dépôt et à la diffusion de documents scientifiques de niveau recherche, publiés ou non, émanant des établissements d'enseignement et de recherche français ou étrangers, des laboratoires publics ou privés.

# Lamb wave attenuation in a rough plate. I. Analytical and experimental results in an anisotropic plate

Cite as: J. Appl. Phys. **104**, 074908 (2008); <https://doi.org/10.1063/1.2979850>

Submitted: 06 November 2007 • Accepted: 20 July 2008 • Published Online: 03 October 2008

Catherine Potel, Damien Leduc, Bruno Morvan, et al.



View Online



Export Citation

## ARTICLES YOU MAY BE INTERESTED IN

[Lamb wave attenuation in a rough plate. II. Analytical and numerical results in a fluid plate](#)  
Journal of Applied Physics **104**, 074909 (2008); <https://doi.org/10.1063/1.2979851>

[The measurement of  \$A\_0\$  and  \$S\_0\$  Lamb wave attenuation to determine the normal and shear stiffnesses of a compressively loaded interface](#)

The Journal of the Acoustical Society of America **113**, 3161 (2003); <https://doi.org/10.1121/1.1568754>

[Lamb waves in highly attenuative plastic plates](#)

The Journal of the Acoustical Society of America **104**, 874 (1998); <https://doi.org/10.1121/1.423332>

Lock-in Amplifiers  
up to 600 MHz



Zurich  
Instruments



## Lamb wave attenuation in a rough plate. I. Analytical and experimental results in an anisotropic plate

Catherine Potel,<sup>1,4,a)</sup> Damien Leduc,<sup>2,4</sup> Bruno Morvan,<sup>2,4</sup> Claude Depollier,<sup>1,4</sup>  
Anne-Christine Hladky-Hennion,<sup>3,4</sup> Jean-Louis Izbicki,<sup>2,4</sup> Pascal Pareige,<sup>2,4</sup> and  
Michel Bruneau<sup>1,4</sup>

<sup>1</sup>Laboratoire d'Acoustique de l'Université du Maine (LAUM) UMR CNRS 6613, 72085 Le Mans, France

<sup>2</sup>Laboratoire d'Ondes et Milieux Complexes (LOMC) FRE CNRS 3112, Université du Havre,  
76600 Le Havre-France

<sup>3</sup>Institut d'Electronique, de Microélectronique et de Nanotechnologie (IEMN), UMR CNRS 8520, 59046  
Lille, France

<sup>4</sup>Fédération Acoustique du Nord-Ouest, (FANO) FR CNRS 3110, France

(Received 6 November 2007; accepted 20 July 2008; published online 3 October 2008)

The characterization of bounded roughened surfaces before applying adhesive joint, in order to detect poor cohesive and adhesive properties, remains difficult. Earlier studies based on analysis of surface wave (Rayleigh waves or Scholte waves) are not really adapted to the characterization of such surfaces. Guided acoustic waves, i.e., Lamb waves, turn out to be the best adapted kind of waves to characterize this roughness when plates are bounded together. It is the aim of this paper to provide analytical and experimental approaches to analyze the behavior of Lamb waves propagating inside plates with a rough surface (small perturbations). First, experimental results of the attenuation effects are given on roughened glass plates. Second, the attenuation factor of the Lamb wave in an anisotropic rough solid plate is calculated through a complex analytical model of the dispersion equation which accounts for the effect of the power spectrum density of the rough profile (including the effect of the statistical roughness parameters). © 2008 American Institute of Physics. [DOI: 10.1063/1.2979850]

### I. INTRODUCTION

Nowadays, the characterization of bounded roughened surfaces before applying adhesive joint, in order to detect poor cohesive and adhesive properties, remains very difficult<sup>1</sup> although it was the subject of studies presented in the literature.<sup>2–8</sup> In order to improve the bonding quality, the bonding surfaces are usually roughened before applying adhesive joints. Despite the extensive use of ultrasonic waves in other areas of nondestructive testing, a relatively small number of studies have been reported on the measurement of the influence of the surface roughness on the propagation of waves. Moreover, in order to characterize the interfaces, these studies usually lie on the analysis of surface waves (Rayleigh waves or Scholte waves).<sup>8–12</sup> The characterization of the quality of adhesive joints cannot be carried out with this kind of surface waves because the joint is inside the plates bounded together. For this reason, the guided acoustic waves (Lamb waves) turn out to be the best adapted kind of wave to characterize the adhesive properties. Consequently, the characterization of the roughness of the plates before applying adhesive joints (essential for the prediction of the adhesive properties), by making use of the same kind of waves, is quite obvious.

The interaction of bulk acoustic guided waves with rough surfaces, owing to their interest in many works, has been dedicated to several applications, especially in optics,

electromagnetism, and acoustics. The diffraction of acoustic waves by a periodically or randomly corrugated surface has been a hot topic for many years. More specifically, the derivation of the characteristics of elastic Lamb waves propagating in solid plates with rough surfaces, making use of phase screen approximation or using the random process theory (in the frame of a small perturbation approximation), has been published during the last decade. The phase screen approximation<sup>13–15</sup> permits to explain the attenuation phenomenon of Lamb waves when propagating along the plate, but it assumes that the roughness can be characterized only by average parameters, neglecting the important effects due to the spatial periods (which always appear in the roughness profile, even if this profile is “randomly” created). The random process theory (assuming a small perturbation approximation)<sup>16,17</sup> involves scattering amplitude matrices (taking into account the shape profile by means of statistical averaged profile periods). It leads to a complex formulation, which would need to be made more tractable so that the comparison between the theoretical and experimental results could become more accessible. Therefore, analytical model concerning only the propagation of guided, compressional acoustic waves,<sup>18</sup> or Finite Element Method (FEM) simulation of Lamb waves in plates with periodic triangular corrugations<sup>19,20</sup> have been carried out, and the results have been compared with experimental one.

In many respects, the work presented in the present paper is an extension of the results contained in Refs. 13–20 and communications linked to them,<sup>21,22</sup> leading to comparisons between analytical and experimental results. It is con-

<sup>a)</sup> Author to whom correspondence should be addressed. Tel.: 33 2 43 83 36 17. FAX: 33 2 43 83 35 20 Electronic mail: catherine.potel@univ-lmans.fr.

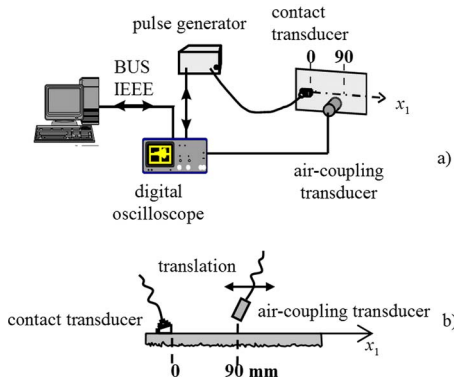


FIG. 1. (Color online) Experimental setup.

cerned with both experimental effects of surface roughness on the propagation of Lamb waves in a corrugated plate (Sec. II) and an analytical model of the dispersion equation leading to results for the attenuation factor when Lamb waves propagate in an anisotropic rough plate. This model takes into account the effect of the power spectrum density (PSD) of the rough profile and includes the effect of the statistical roughness parameters (Secs. III and IV).

## II. EXPERIMENTS

Four glass plates with different kinds of roughness on only one side are experimentally investigated. First, the experimental setup used is presented (Sec. II A). Then the different samples are described, highlighting the spatial periods of the rough profile (Sec. II B). Finally, experimental Lamb wave characteristics are extracted from measured signals (Sec. II C).

### A. Experimental setup

The experimental setup is reported in Fig. 1. A pulse generator delivers a very short pulse voltage (about 300 V during 300 ns) to an emitting contact piezocomposite transducer (central frequency equal to 2.25 MHz). Lamb waves are generated in a plate by the wedge method.<sup>23</sup> The receiving transducer is an air-coupling piezoelectric transducer (central frequency equal to 2 MHz, bandwidth about 700 kHz at  $-3$  dB). The emitting and receiving transducers are both set on the nonrough side of the plate [Fig. 1(b)]. The emitting transducer remains unmoved while the receiving transducer is translated along the propagation direction ( $x_1$ ) of Lamb waves. The displacement amplitudes are collected from  $x_1=10$  mm to  $x_1=90$  mm by 0.1 mm step (the origin  $x_1=0$  corresponds to the wedge position). For each position of the air-coupling transducer, a 200  $\mu$ s signal is acquired on 10 000 points by 0.02  $\mu$ s step. In order to improve the signal to noise ratio, an average of 1000 successive shots is performed.

TABLE I. Characteristics of the isotropic glass: thickness  $d$ , density  $\rho$ , and longitudinal and shear velocities  $V_L$  and  $V_T$ .

$d$ (mm)	$\rho$ (kg m <sup>-3</sup> )	$V_L$ (m s <sup>-1</sup> )	$V_T$ (m s <sup>-1</sup> )
5	5000	5825	3485

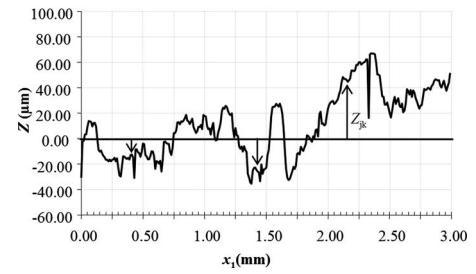


FIG. 2. Example of a rough profile (shot blasted plate).

### B. Spatial periods of the rough profile

The studied samples are four isotropic glass plates with 200 mm sides and 5 mm thickness. The glass density  $\rho$  and the longitudinal and shear velocities ( $V_L$  and  $V_T$ , respectively) are reported in Table I. Three plates are processed in order to obtain a rough surface on one side only. The fourth plate is not processed and thus is used as a reference plate.

Two quite different techniques are used to create surface roughness: sanding and shot blasting. The plate surface topographies are obtained by means of an optical surface profiler. To evaluate the roughness amplitude, statistic parameters  $R_a$  (roughness average) and  $R_q$  (root mean square roughness) are used.<sup>24</sup> Their mathematical expression is defined as follows:

$$R_a = \frac{1}{MN} \sum_{j=1}^M \sum_{i=1}^N |Z_{ij}| \quad (1)$$

and

$$R_q = \frac{1}{MN} \sqrt{\sum_{j=1}^M \sum_{i=1}^N Z_{ij}^2}, \quad (2)$$

where height deviations  $Z_{ij}$  are measured from the mean surface and  $M$  and  $N$  are the numbers of data points in each direction of the array (see Fig. 2 for an example of a rough profile for the shot blasted plate). These parameters cover a large range of roughness and are given in Table II for each plate.

The spatial periods  $\Lambda$  appearing in the rough profile are other characteristics of roughness, which are useful to investigate the propagation phenomena. These spatial periods are determined by using the PSD of each profile (i.e., the Fourier Transform of the autocorrelation function). Experimentally, the PSD is determined from a ( $5 \times 5$  mm<sup>2</sup>) sample, which is divided into 500 lines and 500 rows. The sum of the PSD of all the lines (respectively, rows) gives the PSD for lines (respectively, rows). They are depicted as functions of the spatial period  $\Lambda$  in Figs. 3 for the shot-blasted plate, showing

TABLE II. Roughness statistic parameters for the four glass plates.

Glass plate	$R_a$ ( $\mu$ m)	$R_q$ ( $\mu$ m)
Nontreated	<0.01	<0.01
Sanded	4.8	6.0
Shot blasted	23.3	29.8
Strong shot blasted	52.4	67.4

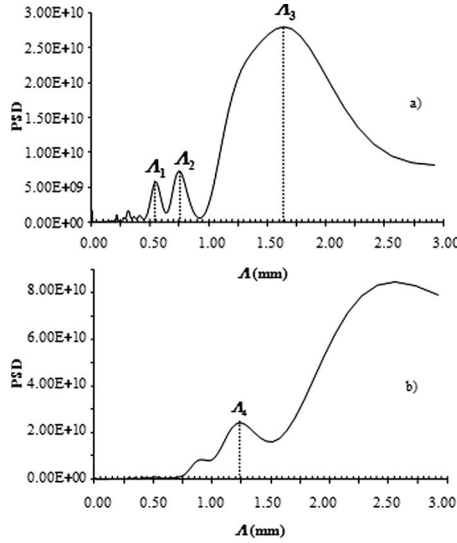


FIG. 3. PSD of a sample of a shot blasted plate (a) average of lines, (b) average of rows.  $\Lambda_1=0.546$  mm,  $\Lambda_2=0.745$  mm,  $\Lambda_3=1.640$  mm, and  $\Lambda_4=1.22$  mm.

that the PSD for lines [Fig. 3(a)] does not present the same maxima as the PSD for rows [Figs. 3(b)]. The presence of several maxima indicates that several main spatial periods  $\Lambda$  coexist in the rough profile (those which will be used subsequently are denoted  $\Lambda_i$ ,  $i=1, \dots, 4$ ). The spatial period  $\Lambda$  is an important parameter, regarding the propagation of Lamb waves [see Part II (Ref. 25)].

### C. Experimental results

Let us note  $k_{1T}$  the projection of the wavenumber vector on the  $x_1$ -axis, its real and imaginary parts being respectively denoted  $k'_{1T}$  and  $k''_{1T}$ ,

$$k_{1T} = k'_{1T} + ik''_{1T}. \quad (3)$$

The results of the experiments described in Sec. II A allow, after some signal analysis, to extract the characteristics for each Lamb mode, for each plate, phase velocities (related to  $k'_{1T}$ ) and attenuation (related to  $k''_{1T}$ ). As expected, the experimental phase velocities corresponding to rough plates are very close to those corresponding to the reference smooth plate.<sup>9,20</sup> As a consequence, they are not relevant for characterizing the effect of the roughness on the propagation of Lamb waves.

The displacement amplitudes of each Lamb mode as a function of  $x_1$  are experimentally obtained by means of a spatial short time Fourier transform. Let us focus on the shot blasted plate (see Fig. 4, other results for the other plates can be found in Ref. 20). Three Lamb modes are studied: symmetric mode  $S_1$  and antisymmetric modes  $A_1$  and  $A_2$ . The imaginary part  $k''_{1T}$ , related to the attenuation of a Lamb mode, which is due to three effects, the effect of the surrounding fluid, the effect of the bounded nature of the ultrasonic beam, and the intrinsic phenomena inside the plate (here the roughness), is obtained from the slope of the logarithm of the experimental curves shown in Fig. 4. Assuming that, for a given Lamb mode, these effects on the imaginary part  $k''_{1T}$  are added the ones to the others, the imaginary part

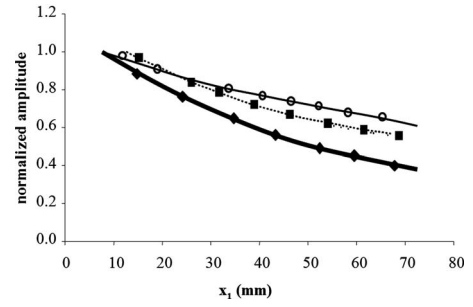


FIG. 4. Experimental normalized displacement amplitudes in a rough shot blasted plate, for Lamb modes  $A_2$  ( $fd=10.8$  MHz mm, thick solid line with closed diamonds),  $S_1$  ( $fd=8.7$  MHz mm, dotted line with closed squares),  $A_1$  ( $fd=5.9$  MHz mm, thin solid line with open circles).

$k''_{1T}$ , corresponding only to the attenuation due to the roughness can be deduced from the following formula:

$$k''_{1T} = k''_{1T} + k''_{1\text{ref}}, \quad (4)$$

where the imaginary part  $k''_{1\text{ref}}$  corresponds to the attenuation of the Lamb mode for the roughless plate (thus only taking into account the effects of the surrounding fluid and of the bounded nature of the ultrasonic beam).

Table III reports the experimental imaginary parts  $k''_{1\text{exp}}$ , of Lamb modes  $S_1$ ,  $A_1$ , and  $A_2$ , for each rough plate. It can be observed that for all the modes, the imaginary part  $k''_{1\text{exp}}$  increases with the root mean square roughness  $R_q$  (see Table II).

### III. SHAPE PROFILE MODEL FOR AN ANISOTROPIC ROUGH PLATE: DISPERSION EQUATION

This section aims at providing a three-dimensional model able to predict the characteristics (in particular the intrinsic wavenumber  $k_1 = k'_1 + ik''_1$ ) of the Lamb modes, which propagate in an anisotropic rough solid plate in vacuum. Assuming small roughness, the dispersion equation for Lamb modes is the same as that for the smooth plate except for an additional perturbation term. The results provided by the resolution of this equation are given in Sec. IV. It should be noted that this model is a monomode approach (only one

TABLE III. Theoretical wavenumber  $k_{10}$  of the smooth plate, experimental imaginary part  $k''_{1\text{exp}}$  of the wavenumber (multiplied by thickness  $d$  of the plate) for each rough plate, and the corresponding theoretical spatial period  $\Lambda_{\text{theor}}$ , which gives a theoretical  $k''_{1\text{exp}}$  equal to the experimental one, for three Lamb modes  $A_1$ ,  $S_1$ , and  $A_2$ .

	Lamb mode	$A_1$	$S_1$	$A_2$
	$fd$ (MHz mm)	5.9	8.7	10.8
	$k_{10}d$	8.8	12.7	14.9
Sanded	$k''_{1\text{exp}}d$	Not measured	0.003	0.006
( $R_q=6.0$ $\mu\text{m}$ )	$\Lambda_{\text{theor}}/d$		0.19	0.474
	$\Lambda_{\text{theor}}$ (mm)		0.95	2.37
Shot blasted	$k''_{1\text{exp}}d$	0.0075	0.025	0.052
( $R_q=29.8$ $\mu\text{m}$ )	$\Lambda_{\text{theor}}/d$	0.052	0.109	0.244
	$\Lambda_{\text{theor}}$ (mm)	0.26	0.546(= $\Lambda_1$ )	1.22(= $\Lambda_4$ )
Strong shot blasted	$k''_{1\text{exp}}d$	0.071	0.1305	0.144
( $R_q=67.4$ $\mu\text{m}$ )	$\Lambda_{\text{theor}}/d$	0.124	0.056	0.034
	$\Lambda_{\text{theor}}$ (mm)	0.62	0.28	0.17

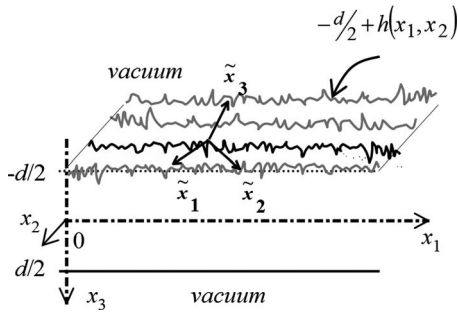


FIG. 5. Anisotropic solid plate in vacuum, with a perturbed boundary surface.

Lamb mode is considered), the purpose being to show how the propagation of a given mode is affected by the roughness.

## A. Geometry of the medium assumptions

The anisotropic plate of Fig. 5 is assumed to be bounded by two parallel planes, only one of them having two-dimensional shape perturbation (three-dimensional geometry). The anisotropic plate with regularly shaped (smooth) surfaces  $x_3 = -d/2$  and  $x_3 = +d/2$  is characterized by its thickness  $d$ , its density  $\rho$ , and its  $(6 \times 6)$  elastic constant matrix  $\mathbf{c}_{\alpha\beta}$ . The boundary surface  $x_3 = -d/2 + h(x_1, x_2)$  has a weak shape variation  $h(x_1, x_2)$  around the plane  $x_3 = -d/2$ . The slopes  $h'_1 = \partial h / \partial x_1$  and  $h'_2 = \partial h / \partial x_2$  are also assumed to be small.

It is worth noting that in the experiment, the rough plate is surrounded by a fluid and the ultrasonic beam is bounded laterally, but in the model, the plate is in vacuum, and the waves propagating in the plate are assumed to be plane waves.

In the problem addressed below, only one Lamb mode is considered (monomode approach). It is worth noting that an intermodal approach is considered in the second part of the paper.

### 1. Change of basis

As the boundary conditions satisfied by the acoustic field on the perturbed surface of the plate are given by the requirement that the stress vector (linked to the normal to the interface) vanishes at every point of the boundary, the local basis  $\tilde{\mathbf{B}} = (\tilde{\mathbf{x}}_1, \tilde{\mathbf{x}}_2, \tilde{\mathbf{x}}_3)$  has to be considered (see Fig. 5),  $\tilde{\mathbf{x}}_3$  being the normal vector to the rough upper surface. The coefficients  $\Xi_{ij}$  of the change-of-basis matrix  $\Xi$  from the Cartesian basis  $\mathbf{B} = (\mathbf{x}_1, \mathbf{x}_2, \mathbf{x}_3)$  (associated to the corresponding upper smooth surface) to the local basis  $\tilde{\mathbf{B}}$ , are such as

$$\Xi = \begin{bmatrix} 1/N_1 & 0 & -h'_1/N_3 \\ 0 & 1/N_2 & -h'_2/N_3 \\ h'_1/N_1 & h'_2/N_2 & 1 \end{bmatrix}, \quad (5)$$

where

$$N_1 = \sqrt{1 + h_1'^2}, \quad (6a)$$

$$N_2 = \sqrt{1 + h_2'^2}, \quad (6b)$$

and

$$N_3 = \sqrt{1 + h_1'^2 + h_2'^2}. \quad (6c)$$

## 2. Stress tensor in the local basis $\tilde{\mathbf{B}}$

Note  $\tilde{\sigma}_{ij}$  and  $\sigma_{k\ell}$  the coefficients of the stress tensors expressed, respectively, in the local basis  $\tilde{\mathbf{B}}$  [linked to each point  $M(\mathbf{x})$  of the surface  $x_3 = -d/2 + h(x_1, x_2)$  and in the Cartesian basis  $\mathbf{B}$ ]. These coefficients  $\tilde{\sigma}_{ij}$  and  $\sigma_{k\ell}$  are linked together by the tensor formula

$$\tilde{\sigma}_{ij} = \Xi_{ik} \Xi_{j\ell} \sigma_{k\ell}, \quad (7)$$

which amounts to writing the matrix relation

$$\tilde{\boldsymbol{\sigma}}(x_1, x_2, x_3) = \mathbf{J} \boldsymbol{\sigma}(x_1, x_2, x_3), \quad (8)$$

where  $\mathbf{J}$  is a  $(3 \times 6)$  matrix given in Appendix A,  $\tilde{\boldsymbol{\sigma}}(x_1, x_2, x_3) = (\tilde{\sigma}_{33}, \tilde{\sigma}_{23}, \tilde{\sigma}_{13})^T$  and  $\boldsymbol{\sigma}(x_1, x_2, x_3) = (\sigma_{11}, \sigma_{22}, \sigma_{33}, \sigma_{23}, \sigma_{13}, \sigma_{12})^T$  are, respectively, the  $(3 \times 1)$  column vector depending on the three components of the stress vector linked to vector  $\tilde{\mathbf{x}}_3$  normal to the upper rough surface and the  $(6 \times 1)$  column vector depending on the six components of the stress tensor, where  $T$  denotes the transpose operation.

Introducing the slowness vector  ${}^{(\eta)}\mathbf{m}$  of the monochromatic plane wave  $(\eta)$  in the plate [its components on the Cartesian basis  $\mathbf{B}$  being denoted  $m_1, m_2$  and  ${}^{(\eta)}m_3$ ] the total particle displacement vector can be written as

$$\mathbf{u}(\mathbf{x}; t) = \sum_{\eta=1}^6 {}^{(\eta)}a {}^{(\eta)}\mathbf{P} e^{-i\omega({}^{(\eta)}\mathbf{m} \cdot \mathbf{x} - t)}, \quad (9)$$

where  ${}^{(\eta)}a$  and  ${}^{(\eta)}\mathbf{P}$  are the displacement amplitude and the polarization vector of wave  $(\eta)$ , respectively, and where  $\omega$  is the angular frequency of the waves.

Hooke's law<sup>26</sup> allows to express the stress tensor in the Cartesian basis  $\boldsymbol{\sigma}(x_1, x_2, x_3)$  as a function of the  $(6 \times 1)$  column vector  $\mathbf{A} = ({}^{(1)}a, {}^{(2)}a, {}^{(3)}a, {}^{(4)}a, {}^{(5)}a, {}^{(6)}a)^T$  [which depends on the six displacement amplitudes  ${}^{(\eta)}a$ ] as follows, the factor  $\{-i\omega \exp[-i\omega(m_1 x_1 + m_2 x_2 - t)]\}$  being omitted,

$$\boldsymbol{\sigma}(x_1, x_2, x_3) = \mathbf{D}\mathbf{H}(x_3)\mathbf{A}, \quad (10)$$

where  $(6 \times 6)$  matrix  $\mathbf{D}$  only depends on the elastic constant matrix  $\mathbf{c}_{\alpha\beta}$ , of components  $m_1$  and  $m_2$ , respectively, on the  $x_1$ -axis and  $x_2$ -axis of the slowness vector  ${}^{(\eta)}\mathbf{m}$  [they are identical for all the waves  $(\eta)$  due to the boundary conditions written for any  $x_1$  and for any  $x_2$ ] and of the polarization vector  ${}^{(\eta)}\mathbf{P}$  (see Appendix B), and where the  $(6 \times 6)$  matrix  $\mathbf{H}(x_3)$  is a diagonal matrix

$$\mathbf{H}(x_3) = \text{diag}[\exp(-i\omega {}^{(\eta)}m_3 x_3)]. \quad (11)$$

Finally, substituting Eq. (10) into Eq. (8) leads to

$$\tilde{\boldsymbol{\sigma}}(x_1, x_2, x_3) = \mathbf{J}\mathbf{D}\mathbf{H}(x_3)\mathbf{A} = \mathbf{N}(x_3)\mathbf{A}, \quad (12)$$

omitting factor  $\{-i\omega \exp[-i\omega(m_1 x_1 + m_2 x_2 - t)]\}$ .

## B. Second order expansion of stress vector

The second order expansion of the stress vector as a function of the three parameters  $h'_1$ ,  $h'_2$ , and  $h$  is presented in two steps. The first one as a function of  $h'_1$  and  $h'_2$  (through the matrix  $\mathbf{J}$ ) and the second one as a function of  $h$  (through matrix  $\mathbf{H}(x_3)$ ) around  $x_3 = -d/2$ .

### 1. Second-order expansion of matrix $\mathbf{J}$ as a function of $h'_1$ and $h'_2$

A second-order expansion of all the coefficients of the change-of-basis matrix  $\Xi$  given by Eq. (5) permits to express the  $(3 \times 6)$  matrix  $\mathbf{J}$  as a linear combination of six matrices:

$$\mathbf{J} \approx \mathbf{J}_0 + h'_1 \mathbf{J}_1 + h'_2 \mathbf{J}_2 + h'_1 h'_2 \mathbf{J}_3 + h_1'^2 \mathbf{J}_4 + h_2'^2 \mathbf{J}_5, \quad (13)$$

where the six matrices  $\mathbf{J}_k$ ,  $k=0, \dots, 5$ , are given in Appendix A.

### 2. Second-order expansion of stress vector $\tilde{\sigma}(x_1, x_2, x_3)$ as a function of $h$

As the boundary surface  $x_3 = -d/2 + h(x_1, x_2)$  has a weak variation  $h(x_1, x_2)$  around the plane  $x_3 = -d/2$ , the matrix  $\mathbf{H}(x_3)$  is expanded in series, and then the matrix  $\tilde{\sigma}(x_1, x_2, x_3)$ , at a second order as a function of  $h$  around this plane.

Using Taylor's formula, it is easy to obtain the following expansion:

$$\mathbf{H}(-d/2 + h) \approx \mathbf{H}_0^- + h\mathbf{H}_1^- + h^2\mathbf{H}_2^-, \quad (14)$$

where matrices  $\mathbf{H}_0^-$ ,  $\mathbf{H}_1^-$ , and  $\mathbf{H}_2^-$  are three diagonal matrices given by

$$\mathbf{H}_0^- = \text{diag}\{\exp[i\omega^{(\eta)} m_3 d/2]\}, \quad (15a)$$

$$\mathbf{H}_1^- = \text{diag}\{-i\omega^{(\eta)} m_3 \exp[i\omega^{(\eta)} m_3 d/2]\}, \quad (15b)$$

and

$$\mathbf{H}_2^- = \text{diag}\left\{-\frac{1}{2}\omega^{2(\eta)} m_3^2 \exp[i\omega^{(\eta)} m_3 d/2]\right\}. \quad (15c)$$

Substituting Eq. (14) into Eq. (12) yields to a second-order expansion of matrix  $\mathbf{N}(x_3)$  as a function of  $h$  [involved in the stress vector  $\tilde{\sigma}(x_1, x_2, x_3)$  through Eq. (12)],

$$\mathbf{N}(-d/2 + h) \approx \mathbf{J}\mathbf{D}\mathbf{H}_0^- + h\mathbf{J}\mathbf{D}\mathbf{H}_1^- + h^2\mathbf{J}\mathbf{D}\mathbf{H}_2^-. \quad (16)$$

### 3. Approximate expression of stress vector $\tilde{\sigma}(x_1, x_2, x_3)$ as a function of $h$ , $h'_1$ and $h'_2$

Substituting Eq. (13) into Eq. (16) yields finally to an approximate expression of matrix  $\mathbf{N}(x_3)$  around the plane  $x_3 = -d/2$ . This expansion is the sum of 18 matrices, the zero-order being  $\mathbf{J}_0\mathbf{D}\mathbf{H}_0^-$ ,

$$\begin{aligned} \mathbf{N}(-d/2 + h) \approx & \mathbf{J}_0\mathbf{D}\mathbf{H}_0^- + h'_1\mathbf{J}_1\mathbf{D}\mathbf{H}_0^- + h'_2\mathbf{J}_2\mathbf{D}\mathbf{H}_0^- \\ & + h'_1 h'_2 \mathbf{J}_3\mathbf{D}\mathbf{H}_0^- + h_1'^2 \mathbf{J}_4\mathbf{D}\mathbf{H}_0^- + h_2'^2 \mathbf{J}_5\mathbf{D}\mathbf{H}_0^- \\ & + h\mathbf{J}_0\mathbf{D}\mathbf{H}_1^- + h^2\mathbf{J}_0\mathbf{D}\mathbf{H}_2^- + h(h'_1\mathbf{J}_1 + h'_2\mathbf{J}_2 \\ & + h'_1 h'_2 \mathbf{J}_3 + h_1'^2 \mathbf{J}_4 + h_2'^2 \mathbf{J}_5)\mathbf{D}(\mathbf{H}_0^- + h\mathbf{H}_1^-). \end{aligned} \quad (17)$$

The final expansion of stress vector  $\tilde{\sigma}(x_1, x_2, x_3)$  around the plane  $x_3 = -d/2$  is obtained by reporting Eq. (17) into Eq. (12).

## C. Boundary conditions

Since the plate is in vacuum, the stress vector linked to the normal to the interfaces vanishes,

$$\tilde{\sigma}(x_1, x_2, -d/2 + h) = 0, \quad \forall x_1, \quad \forall x_2, \quad (18a)$$

$$x_3 = -d/2 + h(x_1, x_2),$$

$$\hat{\sigma}(x_1, x_2, +d/2) = 0, \quad \forall x_1, \quad \forall x_2, \quad x_3 = +d/2, \quad (18b)$$

where  $\hat{\sigma}(x_1, x_2, x_3) = (\sigma_{33}, \sigma_{23}, \sigma_{13})^T$  is the  $(3 \times 1)$  column vector depending on the three components of the stress vector linked to the normal vector  $\mathbf{x}_3$  to the lower surface, i.e., using Eq. (10),

$$\hat{\sigma}(x_1, x_2, x_3) = \mathbf{J}_0\mathbf{D}\mathbf{H}(x_3)\mathbf{A}, \quad (19)$$

omitting factor  $\{-i\omega \exp[-i\omega(m_1 x_1 + m_2 x_2 - t)]\}$ .

The boundary conditions (18a) and (18b) lead to a sixth-order homogeneous system of equations,

$$\mathbf{M}\mathbf{A} = \mathbf{0}, \quad (20)$$

where  $\mathbf{M}$  is a  $(6 \times 6)$  matrix of the form

$$\mathbf{M} = \begin{bmatrix} \mathbf{N}(-d/2 + h) \\ \mathbf{J}_0\mathbf{D}\mathbf{H}_0^+ \end{bmatrix}, \quad (21)$$

with

$$\mathbf{H}_0^+ = \mathbf{H}(x_3 = +d/2) = \text{diag}[\exp(-i\omega^{(\eta)} m_3 d/2)]. \quad (22)$$

Substituting the expansion (17) as a function of  $h$ ,  $h'_1$ , and  $h'_2$  into Eq. (21) leads to the following expansion of matrix  $\mathbf{M}$ :

$$\mathbf{M} \approx \mathbf{M}_0 + \delta\mathbf{M}, \quad (23)$$

where matrix  $\mathbf{M}_0$  corresponds to the homogeneous system of equations, written for regularly shaped (smooth) interfaces, given by

$$\mathbf{M}_0 = \begin{bmatrix} \mathbf{J}_0\mathbf{D}\mathbf{H}_0^- \\ \mathbf{J}_0\mathbf{D}\mathbf{H}_0^+ \end{bmatrix}, \quad (24)$$

and where  $\delta\mathbf{M}$  is the sum of seventeen matrices given in Appendix C.

## D. Dispersion equation

The homogeneous system (20) has nonzero solution only if the determinant  $\det \mathbf{M}$  of matrix  $\mathbf{M}$  is equal to zero, leading to the dispersion equation for Lamb modes, which can be written in the form

$$\det \mathbf{M} = F(k_1, \omega) = 0, \quad (25)$$

where  $k_1$  is the projection of the wavenumber vector on the  $x_1$ -axis, its real and imaginary parts being denoted  $k_1'$  and  $k_1''$ , respectively. The expression (23) of matrix  $\mathbf{M}$  can be written as

$$\mathbf{M} \approx \mathbf{M}_0 + \delta\mathbf{M} = \mathbf{M}_0(\mathbf{I} + \mathbf{M}_0^{-1}\delta\mathbf{M}), \quad (26)$$

where  $\mathbf{M}_0^{-1}$  is the inverse matrix of  $\mathbf{M}_0$  and  $\mathbf{I}$  is the identity matrix. A first-order expansion of Eq. (8) permits the determinant of  $\mathbf{M}$  to be expressed as follows:

$$\det \mathbf{M} \approx \det \mathbf{M}_0 + \text{Tr}(\tilde{\mathbf{M}}_0 \delta\mathbf{M}), \quad (27)$$

where  $\text{Tr}(\mathbf{X})$  and  $\tilde{\mathbf{X}}$  are the trace and the adjoint of matrix  $\mathbf{X}$ , respectively. Equation (25) can thus be written in the form

$$F(k_1, \omega) \approx F_0(k_1, \omega) + \delta F(k_1, \omega) = 0, \quad (28)$$

where

$$F_0(k_1, \omega) = \det \mathbf{M}_0, \quad (29a)$$

and

$$\delta F(k_1, \omega) = \text{Tr}(\tilde{\mathbf{M}}_0 \delta\mathbf{M}). \quad (29b)$$

The function  $F_0(k_1, \omega)$  corresponds to the dispersion equation for classical Lamb modes in a plate with plane surfaces. In this case, for a given angular frequency  $\omega$ , the solution is real and is denoted  $k_{1_0}$ . The roughness of the stress-free boundary induces a small complex perturbation  $\delta k_1 = \delta k'_1 + i\delta k''_1$ . Thus, it is assumed that for a given angular frequency  $\omega$ , the solution  $k_1$  of the dispersion Eq. (25) can be written as

$$k_1 = k_{1_0} + \delta k_1, \quad (30)$$

the real and imaginary parts of which being related to the shift frequency and to the attenuation of the wave, respectively. It should be noted that the real part  $\delta k'_1$  of the small complex perturbation  $\delta k_1$  is much smaller than  $k_{1_0}$ .

### E. Physical interpretation

Though there is no absorption in the anisotropic medium, the wavenumber of the Lamb wave, which propagates in the rough plate, is complex, meaning that the corresponding amplitude decreases as a function of  $x_1$ , which has already been observed experimentally (see Sec. II C).

In fact, the mechanism of decay of a Lamb mode may be explained as follows (Fig. 6). When the interfaces are smooth [Fig. 6(a)], for a given pulsation  $\omega$  and a given wavenumber  $k_{1_0}$ , phase matching occurs on the two parallel interfaces between the six plane waves. When the plate is rough [Fig. 6(b)], this phase matching does not occur in the same manner. In other words, it can be said that the initial Lamb mode is scattered by the roughness. These scattered waves combine together to create other Lamb modes. In other words, when impacting the roughness, the main Lamb mode (0) with wavenumber  $k_{1_0}$  is scattered, creating other Lamb modes with different wavenumbers  $k_a, k_b, k_c, \dots$ . Thus, by coupling at the rough interface, there is an energy transfer between all Lamb modes (0), (a), (b), (c),  $\dots$ , which can propagate in the plate. Because the energy given by the source is only provided to the main Lamb mode (0), statistically, it is this mode that distributes acoustic energy to the other modes; thus, its amplitude decreases.

As the present model is a monomode approach, Lamb mode (0), the problem (20), which leads to the dispersion Eq.

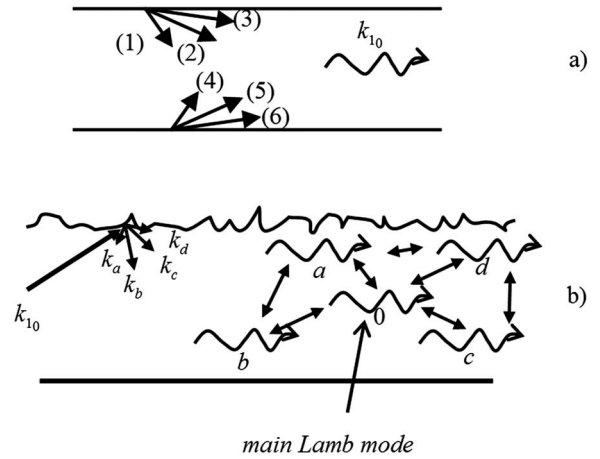


FIG. 6. Schematic view of energy transfers by coupling on the roughness. (a) propagation of the main Lamb mode (0) in the plate with smooth interfaces, (b) scattering of the main Lamb mode on the roughness and energy transfers between all the Lamb modes created by coupling.

(25) or Eq. (28), is representative of its scattering due to the roughness and thus of its loss of energy (through energy transfer to other modes), which is therefore characterized by a complex perturbation  $\delta k_1$  of the wavenumber  $k_{1_0}$  corresponding to the main Lamb mode (0) without roughness.

Results presented below in Part II (Ref. 25) justify this physical interpretation, in the simple case of a fluid plate with the same shape profile model but in the frame of an intermodal approach.

## IV. SHAPE PROFILE MODEL FOR AN ISOTROPIC ROUGH PLATE: ATTENUATION FACTOR

This section aims at providing theoretical results coming from the shape profile model developed in Sec. III and to compare them with the experimental results obtained in Sec. II. When propagating, the Lamb wave is sensitive to effective parameters of the roughness, linked to the statistical parameters  $R_a$  and  $R_q$  and to the spatial periods  $\Lambda$  of the profile, which have to be related to weak parameters, namely the variation  $h$  and the slopes  $h'_1$  and  $h'_2$  (see Sec. IV A). In Sec. IV B, the numerical resolution of the dispersion Eq. (28) is discussed briefly, and the importance of the spatial period of the rough profile is highlighted together with a comparison between theoretical and experimental results.

### A. Effective parameters

For a given angular frequency  $\omega$ , the dispersion Eq. (28) provides a wavenumber  $k_1$  for each abscissa  $(x_1, x_2)$  of the rough profile. It is worth noting that this refinement is consistent with the boundary conditions, which are not self-similar in the  $x_1$  and  $x_2$  directions, but it prevents us from deriving the expected wavenumber, which expresses statistically averaged effects of the roughness. Moreover, it is appropriate to estimate the attenuation factor due to the roughness (given through the imaginary part  $k''_1$  of the wavenumber  $k_1$ ), which would reflect the statistical properties of the roughness expressed by the normalized functions  $R_a$  or  $R_q$  [Eqs. (1) and (2), respectively]. In other words, it is suitable to replace the parameters  $h, h'_1,$  and  $h'_2$  expressing the rough-

ness in expression (28) [through expression (17) of the matrix  $\mathbf{N}$ ] by effective parameters defined as their statistical averaged expressions, namely for example,  $R_q$  for  $h^2$ ,  $R_a/(\Lambda/4)$  for both  $h'_1$  and  $h'_2$ , assuming in this last approximation that the rough profile behaves statistically as a periodic sawtooth profile with spatial period  $\Lambda$  (it appears that the effect of the slopes  $h'_1$  and  $h'_2$  are predominant).

This first approach provides results that must be regarded as qualitative results. In Part II a deeper analysis is provided, but it is limited to longitudinal waves (fluid guide).

It is noteworthy that the effective parameters involved in the dispersion equation are expressed as a function of data easily accessible experimentally, including the spatial periods of the rough profile, which are important parameters, as it will be seen in Sec. IV B and, in Part II (Ref. 25) for the case of a fluid plate.

## B. Solutions of the dispersion equation and results

The numerical resolution of the dispersion Eq. (25) or Eq. (28) leads, for a given angular frequency  $\omega$ , to a complex wavenumber  $k_1 = k'_1 + ik''_1$ . Two methods have been used: the Simplex algorithm<sup>27</sup> and a Taylor expansion (Appendix D).

Though the Simplex algorithm is a very reliable and robust method, it needs a starting point and may sometimes lead to divergent solutions. Moreover, the computation with this algorithm takes several hours when using a 797 MHz Processor 2800 in a usual personal computer. In order to avoid these difficulties, we used a Taylor expansion of the function  $F(k_1, \omega)$  at the second-order of parameter  $\delta k_1$  (see Appendix D for the detailed calculation). The dispersion curves obtained by the second-order Taylor expansion are almost the same as those obtained by the Simplex algorithm. The computation using Taylor expansion takes about only 5 min and there is no lack of convergence, but higher modes (mode  $A_7$  for example) may not be correctly found (it should be noted that the modes are here named as in Ref. 28 for example). Thus, for most of the cases, the second-order Taylor expansion is sufficient to obtain reliable results, but the Simplex algorithm may be useful to punctually confirm some results.

As expected, for the three glass plates (sanded, shot blasted, and strong shot blasted, see Tables I and II and Sec. II B), the real part  $k'_1$  of the wavenumber is very close to the real wavenumber  $k_{10}$  corresponding to classical Lamb waves in a plate with smooth interfaces. As a consequence, the dispersion curves for the real part of the wavenumber, i.e., curves  $k'_1$  as functions of frequency  $f$  [see Fig. 7(a) for the shot blasted plate], are almost the same for all the plates. This theoretical result is in excellent agreement with the experimental results summarized in Sec. II B.<sup>13,20</sup>

As far as the imaginary part  $k''_1$  of the wavenumber is concerned, the results strongly depend on the effective parameters expressing the roughness in expression (28), these parameters being related to the statistical characteristics of the rough profile [expressed by Eqs. (1) and (2)] and, in particular, to a spatial period  $\Lambda$  of the profile (see Sec. IV A). An example of dispersion curves for  $k''_1$  as a function of the frequency is given in Fig. 7(b) for a shot blasted plate with

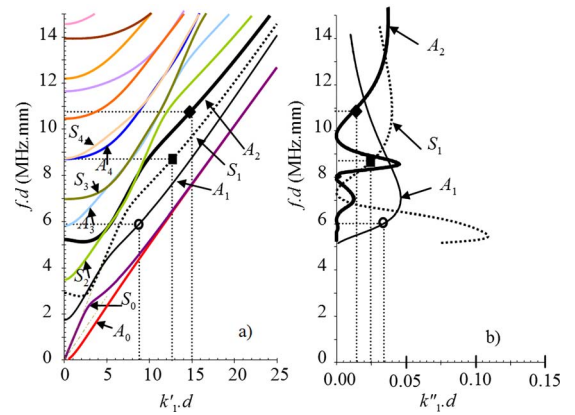


FIG. 7. (Color online) Dispersion curves for Lamb waves in a shot blasted plate ( $\Lambda = \Lambda_1 = 0.546$  mm) obtained by the three-dimensional model and second-order Taylor expansion; (a) real part  $k'_1 d$  as a function of frequency  $f$ , (b) imaginary part  $k''_1 d$  as a function of frequency  $f$ .

$\Lambda = \Lambda_1 = 0.546$  mm (in order to make the figure clearer for the present discussion, the upper modes have been cancelled and the curves have been drawn only in the frequency range of interest).

In order to determine how the imaginary part  $k''_1$  is sensitive to the spatial period  $\Lambda$ , we have studied the variation of product  $k''_1 d$  (where  $d$  is the thickness of the smooth plate) as a function of  $\Lambda/d$  (see Fig. 8 for the shot blasted plate), and with a view to comparing with experimental results, the curves are drawn for three Lamb modes ( $A_1, S_1$ , and  $A_2$ ), in the validity domain i.e., assuming that the slopes  $h'_1$  and  $h'_2$  are small (see Sec. III A). It can be observed that the more the spatial period  $\Lambda$  increases, the less the imaginary part  $k''_1$  is sensitive to  $\Lambda$ . As a consequence, the results will be quite different when taking into account the main spatial periods, which are involved in the PSD of the rough profile. However, there might be several quite different PSDs (and thus several spatial periods) for a given rough profile, depending on the sampling considered [see Sec. II B and Figs. 3(a) and 3(b)]. Therefore, a given Lamb mode can be sensitive to a given spatial period, whereas another Lamb mode will be sensitive to another one. For each rough glass plate, the theoretical spatial period  $\Lambda$ , which gives a perfect matching of the theoretical  $k''_1$  with the experimental  $k''_1$  (denoted  $k''_{1 \text{ exp}}$ ), is reported in Table III. For the shot blasted plate and for mode

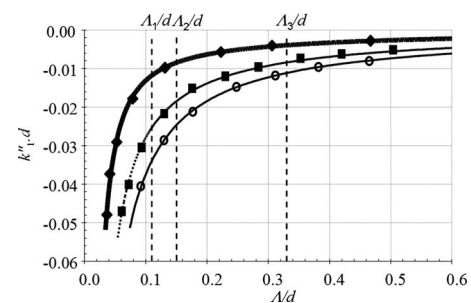


FIG. 8. Theoretical imaginary part  $k''_1$  (multiplied by thickness  $d$  of the plate) as a function of the spatial period  $\Lambda$  (divided by thickness  $d$  of the plate, for a given thickness  $d$ ) of the shot blasted rough profile, for Lamb modes  $A_2$  ( $fd = 10.8$  MHz.mm,  $\lambda/d = 0.42$ , thick solid line with closed diamonds),  $S_1$  ( $fd = 8.7$  MHz.mm,  $\lambda/d = 0.494$ , dotted line with closed squares),  $A_1$  ( $fd = 5.9$  MHz.mm,  $\lambda/d = 0.714$ , thin solid line with open circles).

$S_1$ , this spatial period corresponds to,  $\Lambda_1=0.546$  mm which is found on the PSD of Fig. 3(a), and for mode  $A_2$ , it corresponds to  $\Lambda_4=1.22$  mm [see Fig. 3(b)]. However, for a given spatial period,  $\Lambda_1$  for instance,  $k_1''d=0.0034$  for the mode  $A_1$ , 0.025 for the mode  $S_1$ , and the 0.012 for mode  $A_2$  (see the corresponding closed circle, closed square, and closed diamond, respectively, in Fig. 7).

It can also be observed from Fig. 8 that since the spatial period  $\Lambda$  is inversely proportional to the roughness average  $R_a$  (see Sec. IV A), the more  $R_a$  increases (i.e., the more  $\Lambda$  decreases), the more  $k_1''$  increases. This result is in agreement, for each mode, with the experimental results given in Table III: the experimental imaginary part  $k_1''_{\text{exp}}$  increases with  $R_a$ . It should be noted that for the strong shot blasted plate, the assumption that  $h_1'$  and  $h_2'$  small is no more verified and thus the model is no longer valid.

As a remark, it can be noted that when the condition (phonon relation)

$$2k_1' \pm 2\pi/\Lambda = 0 \quad (31)$$

is satisfied,<sup>18,19</sup> there is a strong coupling between the main Lamb mode and the same Lamb mode created by the scattering on the roughness (this is the case for mode  $A_1$ , with  $\Lambda=\Lambda_3$ ). The phonon relation will be studied with more details in Part II.<sup>25</sup>

## V. CONCLUSION

The motivation for this study was to characterize the influence of a surface roughness on the propagation of waves in anisotropic rough solid plates, having in mind the characterization of the quality of adhesive joints.

Unlike earlier studies based on the analysis of surface waves (Rayleigh waves or Scholte waves), which are not really dedicated to the characterization of surface roughened before applying adhesive joints inside plates bounded to-

gether, the current study uses the much more adapted guided acoustic waves, i.e., Lamb waves. These waves are analyzed in order to sequentially (i) give experimental results of the attenuation effects of the surface roughness on the propagation of several Lamb waves and (ii) calculate the attenuation factor of the Lamb waves due to the roughness in an anisotropic rough solid plate, through a complex analytical model of the dispersion equation (monomode shape profile model).

Consistency between the theoretical and experimental results is reported. As expected, the real part  $k_1'$  of the wave-number  $k_1$  is very close to the real wavenumber  $k_{10}$  corresponding to classical Lamb waves in a plate with smooth interfaces, and the imaginary part  $k_1''$  increases with the roughness average  $R_a$ . This imaginary part also strongly depends on the spatial periods  $\Lambda$ , which appear in the rough profile through its PSD, as verified theoretically. An inter-modal analytical modeling limited to compressional acoustic waves (fluid plate), is done in Part II.<sup>25</sup> From this approach a physical interpretation of several phenomena involved in the presence of rough interface is given. Numerical validation of this modeling is also provided using FEM.

## ACKNOWLEDGMENTS

Support from CNRS through the research group (GDR-2501) is gratefully acknowledged. The authors are grateful to the reviewer for his constructive suggestion to separate the earlier version of this paper in two parts.

## APPENDIX A: EXPRESSIONS OF MATRIX J

Coefficients  $\tilde{\sigma}_{ij}$  and  $\sigma_{k\ell}$  are related by the tensor formula (7) (see Sec. III A 2),

$$\tilde{\sigma}_{ij} = \Xi_{ik} \Xi_{j\ell} \sigma_{k\ell}, \quad (A1)$$

where coefficients  $\Xi_{ik}$  of the change-of-basis matrix  $\Xi$  are given by Eq. (5), in particular,  $\Xi_{21}=\Xi_{12}=0$ .

As a consequence,

$$\mathbf{J} = \begin{bmatrix} \Xi_{31}^2 & \Xi_{32}^2 & \Xi_{33}^2 & 2\Xi_{32}\Xi_{33} & 2\Xi_{31}\Xi_{33} & 2\Xi_{31}\Xi_{32} \\ 0 & \Xi_{22}\Xi_{32} & \Xi_{23}\Xi_{33} & (\Xi_{22}\Xi_{33} + \Xi_{23}\Xi_{32}) & \Xi_{23}\Xi_{31} & \Xi_{22}\Xi_{31} \\ \Xi_{11}\Xi_{31} & 0 & \Xi_{13}\Xi_{33} & \Xi_{13}\Xi_{32} & (\Xi_{11}\Xi_{33} + \Xi_{13}\Xi_{31}) & \Xi_{11}\Xi_{32} \end{bmatrix}. \quad (A2)$$

Substituting Eqs. (5) and (6) into Eq. (A1) and expanding each coefficient at a second order in  $h_1'$  and  $h_2'$  leads to

$$\mathbf{J} \approx \begin{bmatrix} h_1'^2 & h_2'^2 & 1 & 2h_2' & 2h_1' & 2h_1'h_2' \\ 0 & h_2' & -h_2' & 1 - \frac{3}{2}h_2'^2 & -h_1'h_2' & h_1' \\ h_1' & 0 & -h_1' & -h_1'h_2'^2 & 1 - \frac{3}{2}h_1'^2 & h_2' \end{bmatrix}. \quad (A3)$$

This last expression can thus be written as follows:

$$\mathbf{J} \approx \mathbf{J}_0 + h_1'\mathbf{J}_1 + h_2'\mathbf{J}_2 + h_1'h_2'\mathbf{J}_3 + h_1'^2\mathbf{J}_4 + h_2'^2\mathbf{J}_5, \quad (A4)$$

where

$$\mathbf{J}_0 = \begin{bmatrix} 0 & 0 & 1 & 0 & 0 & 0 \\ 0 & 0 & 0 & 1 & 0 & 0 \\ 0 & 0 & 0 & 0 & 1 & 0 \end{bmatrix}, \quad (A5)$$

$$\mathbf{J}_1 = \begin{bmatrix} 0 & 0 & 0 & 0 & 2 & 0 \\ 0 & 0 & 0 & 0 & 0 & 1 \\ 1 & 0 & -1 & 0 & 0 & 0 \end{bmatrix}, \quad (A6)$$

$$\mathbf{J}_2 = \begin{bmatrix} 0 & 0 & 0 & 2 & 0 & 0 \\ 0 & 1 & -1 & 0 & 0 & 0 \\ 0 & 0 & 0 & 0 & 0 & 1 \end{bmatrix}, \quad (A7)$$

$$\mathbf{J}_3 = \begin{bmatrix} 0 & 0 & 0 & 0 & 0 & 2 \\ 0 & 0 & 0 & 0 & -1 & 0 \\ 0 & 0 & 0 & -1 & 0 & 0 \end{bmatrix}, \quad (\text{A8})$$

$$\mathbf{J}_4 = \begin{bmatrix} 1 & 0 & 0 & 0 & 0 & 0 \\ 0 & 0 & 0 & 0 & 0 & 0 \\ 0 & 0 & 0 & 0 & -3/2 & 0 \end{bmatrix}, \quad (\text{A9})$$

$$\mathbf{J}_5 = \begin{bmatrix} 0 & 1 & 0 & 0 & 0 & 0 \\ 0 & 0 & 0 & -3/2 & 0 & 0 \\ 0 & 0 & 0 & 0 & 0 & 0 \end{bmatrix}. \quad (\text{A10})$$

## APPENDIX B: EXPRESSIONS OF MATRIX $\mathbf{D}$

Hooke's law, which relates coefficients  $\sigma_{ij}$  of the stress tensor to the coefficients of the strain tensor [through components  $u_k$  of the displacement vector  $\mathbf{u}$  given by Eq. (9)], can be written as

$$\sigma_{ij} = c_{ijk\ell} \partial u_k / \partial x_\ell, \quad (\text{B1})$$

where  $c_{ijk\ell}(i, j, k, \ell = 1, 2, 3)$  are the coefficients of the rigid elastic fourth-order tensor, related to coefficients  $c_{\alpha\beta}(\alpha, \beta = 1, \dots, 6)$  of the rigid elastic ( $6 \times 6$ ) matrix  $\mathbf{c}_{\alpha\beta}$  by the convention  $\alpha \leftrightarrow (ij)$  and  $\beta \leftrightarrow (k\ell)$ , with

$$1 \leftrightarrow (11), \quad 2 \leftrightarrow (22), \quad 3 \leftrightarrow (33),$$

$$4 \leftrightarrow (23), \quad 5 \leftrightarrow (13), \quad 6 \leftrightarrow (12). \quad (\text{B2})$$

Substituting expression (9) of the displacement vector  $\mathbf{u}$  into Eq. (B1) leads to

$$\sigma_\alpha = \sum_{\eta=1}^6 {}^{(\eta)}a D_{\alpha\eta} e^{-i\omega({}^{(\eta)}m_3 x_3)}, \quad \alpha = 1, \dots, 6, \quad (\text{B3})$$

omitting factor  $\{-i\omega \exp[-i\omega(m_1 x_1 + m_2 x_2 - t)]\}$ , where

$$\begin{aligned} D_{\alpha\eta} = & c_{\alpha 1} m_1 {}^{(\eta)}P_1 + c_{\alpha 2} m_2 {}^{(\eta)}P_2 + c_{\alpha 3} {}^{(\eta)}m_3 {}^{(\eta)}P_3 \\ & + c_{\alpha 4} {}^{(\eta)}m_3 {}^{(\eta)}P_2 + m_2 {}^{(\eta)}P_3 + c_{\alpha 5} {}^{(\eta)}m_3 {}^{(\eta)}P_1 \\ & + m_1 {}^{(\eta)}P_3 + c_{\alpha 4} (m_2 {}^{(\eta)}P_1 + m_1 {}^{(\eta)}P_2) \end{aligned} \quad (\text{B4})$$

are the coefficients of ( $6 \times 6$ ) matrix  $\mathbf{D}$ ,  $m_1$ , and  $m_2$  being the components on  $x_1$ -axis and  $x_2$ -axis of the slowness vector  $\mathbf{m}$  of all the waves ( $\eta$ ), and  ${}^{(\eta)}P_j$  being the components on  $x_j$ -axis of the polarization vector of the wave ( $\eta$ ).

Finally, Eq. (B3) can be written in the following matrix form:

$$\boldsymbol{\sigma}(x_1, x_2, x_3) = \mathbf{DH}(x_3)\mathbf{A}, \quad (\text{B5})$$

omitting factor  $\{-i\omega \exp[-i\omega(m_1 x_1 + m_2 x_2 - t)]\}$ , where matrices  $\mathbf{H}(x_3)$  and  $\mathbf{A}$  are defined in Sec. III A 2.

## APPENDIX C: EXPANSION OF MATRIX $\mathbf{M}$

The expansion of matrix  $\mathbf{M}$  is obtained by substituting the expansion (17) of matrix  $\mathbf{N}(-d/2+h)$  into expression (21) of matrix  $\mathbf{M}$ ,

$$\mathbf{M} \approx \mathbf{M}_0 + \delta\mathbf{M}, \quad (\text{C1})$$

where  $\mathbf{M}_0$  is given by Eq. (24) and  $\delta\mathbf{M}$  by

$$\begin{aligned} \delta\mathbf{M} \approx & h'_1 \mathbf{M}_1 + h'_2 \mathbf{M}_2 + h'_1 h'_2 \mathbf{M}_3 + h_1'^2 \mathbf{M}_4 + h_2'^2 \mathbf{M}_5 + h \mathbf{M}_6 \\ & + h^2 \mathbf{M}_7 + h h'_1 \mathbf{M}_8 + h h'_2 \mathbf{M}_9 + h h'_1 h'_2 \mathbf{M}_{10} + h h_1'^2 \mathbf{M}_{11} \\ & + h h_2'^2 \mathbf{M}_{12} + h^2 h_1' \mathbf{M}_{13} + h^2 h_2' \mathbf{M}_{14} + h^2 h_1' h_2' \mathbf{M}_{15} \\ & + h^2 h_1'^2 \mathbf{M}_{16} + h^2 h_2'^2 \mathbf{M}_{17}. \end{aligned} \quad (\text{C2})$$

The seventeen matrices are given by

$$\mathbf{M}_1 = \begin{bmatrix} \mathbf{J}_1 \mathbf{DH}_0^- \\ \mathbf{0} \end{bmatrix}, \quad \mathbf{M}_2 = \begin{bmatrix} \mathbf{J}_2 \mathbf{DH}_0^- \\ \mathbf{0} \end{bmatrix}, \quad (\text{C3})$$

$$\mathbf{M}_3 = \begin{bmatrix} \mathbf{J}_3 \mathbf{DH}_0^- \\ \mathbf{0} \end{bmatrix}, \quad \mathbf{M}_4 = \begin{bmatrix} \mathbf{J}_4 \mathbf{DH}_0^- \\ \mathbf{0} \end{bmatrix},$$

$$\mathbf{M}_5 = \begin{bmatrix} \mathbf{J}_5 \mathbf{DH}_0^- \\ \mathbf{0} \end{bmatrix}, \quad \mathbf{M}_6 = \begin{bmatrix} \mathbf{J}_0 \mathbf{DH}_1^- \\ \mathbf{0} \end{bmatrix},$$

$$\mathbf{M}_7 = \begin{bmatrix} \mathbf{J}_0 \mathbf{DH}_2^- \\ \mathbf{0} \end{bmatrix}, \quad \mathbf{M}_8 = \begin{bmatrix} \mathbf{J}_1 \mathbf{DH}_1^- \\ \mathbf{0} \end{bmatrix},$$

$$\mathbf{M}_9 = \begin{bmatrix} \mathbf{J}_2 \mathbf{DH}_1^- \\ \mathbf{0} \end{bmatrix}, \quad \mathbf{M}_{10} = \begin{bmatrix} \mathbf{J}_3 \mathbf{DH}_1^- \\ \mathbf{0} \end{bmatrix},$$

$$\mathbf{M}_{11} = \begin{bmatrix} \mathbf{J}_4 \mathbf{DH}_1^- \\ \mathbf{0} \end{bmatrix}, \quad \mathbf{M}_{12} = \begin{bmatrix} \mathbf{J}_5 \mathbf{DH}_1^- \\ \mathbf{0} \end{bmatrix},$$

$$\mathbf{M}_{13} = \begin{bmatrix} \mathbf{J}_1 \mathbf{DH}_2^- \\ \mathbf{0} \end{bmatrix}, \quad \mathbf{M}_{14} = \begin{bmatrix} \mathbf{J}_2 \mathbf{DH}_2^- \\ \mathbf{0} \end{bmatrix},$$

$$\mathbf{M}_{15} = \begin{bmatrix} \mathbf{J}_3 \mathbf{DH}_2^- \\ \mathbf{0} \end{bmatrix}, \quad \mathbf{M}_{16} = \begin{bmatrix} \mathbf{J}_4 \mathbf{DH}_2^- \\ \mathbf{0} \end{bmatrix},$$

$$\mathbf{M}_{17} = \begin{bmatrix} \mathbf{J}_5 \mathbf{DH}_2^- \\ \mathbf{0} \end{bmatrix}.$$

## APPENDIX D: SECOND-ORDER TAYLOR EXPANSION OF THE DISPERSION RELATION FOR LAMB MODES

The dispersion equation for Lamb modes in the rough plate is of the form (see Sec. III D)

$$F(k_1, \omega) = 0, \quad (\text{D1})$$

with

$$F(k_1, \omega) \approx F_0(k_1, \omega) + \delta F(k_1, \omega), \quad (\text{D2})$$

and

$$F_0(k_1, \omega) = 0, \quad (\text{D3})$$

where  $k_1$  is the solution of the dispersion Eq. (D3), for a given pulsation  $\omega$ , for the classical Lamb modes in a plate with smooth interfaces.

It is assumed that, for a given angular frequency  $\omega$ , solution  $k_1$  of Eq. (D2) is of the form

$$k_1 = k_{1_0} + \delta k_1, \quad (\text{D4})$$

where  $\delta k_1$  is a complex number.

### 1. First-order expansion

Using Eq. (D4), function  $F(k_1, \omega)$  can be expanded at the first-order,

$$F(k_1, \omega) \approx F_0(k_{1_0}, \omega) + \delta k_1 \frac{\partial F}{\partial k_1}(k_{1_0}, \omega). \quad (\text{D5})$$

Substituting Eq. (D2) into Eq. (D5) and using Eqs. (D1) and (D3) yields to

$$\delta k_1 \approx -\delta F(k_{1_0}, \omega) / \frac{\partial F}{\partial k_1}(k_{1_0}, \omega), \quad (\text{D6})$$

denoted below  $\delta k_1^{(1)}$ .

### 2. Second-order expansion

Using Eq. (D4), function  $F(k_1, \omega)$  can also be expanded at the second-order. Its vanishing leads to a polynomial function of the second degree in the variable  $\delta k_1$ :

$$(\delta k_1)^2 \frac{\partial^2 F}{\partial k_1^2}(k_{1_0}, \omega) + 2(\delta k_1) \frac{\partial F}{\partial k_1}(k_{1_0}, \omega) + 2\delta F(k_{1_0}, \omega) \approx 0 \quad (\text{D7})$$

which has two roots

$$\delta k_1 \approx -\left[ \frac{\partial F}{\partial k_1}(k_{1_0}, \omega) \pm \delta \right] / \frac{\partial^2 F}{\partial k_1^2}(k_{1_0}, \omega), \quad (\text{D8a})$$

denoted below  $\delta k_1^{(2)}$ , with

$$\delta^2 = \left[ \frac{\partial F}{\partial k_1}(k_{1_0}, \omega) \right]^2 - 2\delta F(k_{1_0}, \omega) \frac{\partial^2 F}{\partial k_1^2}(k_{1_0}, \omega). \quad (\text{D8b})$$

If these two roots have opposite imaginary parts, the physical root corresponds to a decreasing of the Lamb wave, i.e., to  $\text{Im}(\delta k_1^{(2)}) = \delta k_1''^{(2)} < 0$ . If the imaginary parts of the two roots has the same sign, the chosen root is such as its imaginary part  $\delta k_1''^{(2)}$  is the closest to the imaginary part  $\delta k_1''^{(1)}$  coming

from the first-order expansion [see Eq. (D5)].

- <sup>1</sup>C. C. Guyott, P. Cawley, and R. D. Adam, *J. Adhes.* **20**, 129 (1986).
- <sup>2</sup>S. Banerjee and T. Kundu, *J. Acoust. Soc. Am.* **119**, 2006 (2006).
- <sup>3</sup>T. Kundu, S. Banerjee, and K. V. Jata, *J. Acoust. Soc. Am.* **120**, 1217 (2006).
- <sup>4</sup>S. Banerjee and T. Kundu, *Int. J. Solids Struct.* **43**, 6551 (2006).
- <sup>5</sup>J. M. Claeys, O. Leroy, A. Jungman, and L. Adler, *J. Appl. Phys.* **54**, 5657 (1983).
- <sup>6</sup>A. Jungman, L. Adler, J. D. Achenbach, and R. Roberts, *J. Acoust. Soc. Am.* **74**, 1025 (1983).
- <sup>7</sup>K. Mampaert and O. Leroy, *J. Acoust. Soc. Am.* **83**, 1390 (1988).
- <sup>8</sup>W. Lauriks, L. Kelders, and J. F. Allard, *Ultrasonics* **36**, 865 (1998).
- <sup>9</sup>A. A. Maradudin and D. L. Mills, *Ann. Phys.* **100**, 262 (1976).
- <sup>10</sup>J. R. Chamuel, *J. Acoust. Soc. Am.* **83**, 1336 (1988).
- <sup>11</sup>H. Duflo, A. Tinel, and J. Duclos, Proceedings of the IEEE International Ultrasonics Symposium Cannes, Strasbourg, France, 1994, pp. 719–722.
- <sup>12</sup>A. A. Tarasenko, L. Jastrabik, and N. A. Tarasenko, *Eur. Phys. J.: Appl. Phys.* **24**, 3 (2003).
- <sup>13</sup>D. E. Chimenti and O. I. Lobkis, *Ultrasonics* **36**, 155 (1998).
- <sup>14</sup>O. I. Lobkis and D. E. Chimenti, *J. Acoust. Soc. Am.* **102**, 143 (1997).
- <sup>15</sup>O. I. Lobkis and D. E. Chimenti, *J. Acoust. Soc. Am.* **102**, 150 (1997).
- <sup>16</sup>S. Dai and H. Zhang, *Chin. J. Acoust.* **22**, 194 (2003).
- <sup>17</sup>S. Dai and H. Zhang, *Chin. J. Acoust.* **22**, 204 (2003).
- <sup>18</sup>C. Potel and M. Bruneau, *J. Sound Vib.* **313**, 738-759 (2008).
- <sup>19</sup>B. Morvan, A.-C. Hladky-Hennion, D. Leduc, and J. L. Izbicki, *J. Appl. Phys.* **101**, 114906 (2007).
- <sup>20</sup>D. Leduc, B. Morvan, P. Pareige, and J. L. Izbicki, *NDT & E Int.* **37**, 207 (2004).
- <sup>21</sup>C. Potel, D. Leduc, B. Morvan, P. Pareige, J. L. Izbicki, and C. Depollier, Proceedings of the Fifth World Congress on Ultrasonics, Paris, France, 2003, pp. 609–612.
- <sup>22</sup>C. Potel, D. Leduc, B. Morvan, P. Pareige, C. Depollier, and J. L. Izbicki, Proceedings of the Joint Congress CFA/DAGA'047, Strasbourg, 2004, pp. 147–148.
- <sup>23</sup>F. Luppé, J. M. Conoir, M. Ech-Cherif El Kettani, O. Lenoir, J. L. Izbicki, J. Duclos, and B. Poirée, *Acoustic Interactions with Submerged Elastic Structures* (World Scientific, Singapore, 2001), Pt. 3.
- <sup>24</sup>ASME B46, 1-1995, *Surface Texture, Surface Roughness, Waviness and Lay* (American Society of Mechanical Engineers, New York, 1995).
- <sup>25</sup>C. Potel, D. Leduc, B. Morvan, C. Depollier, A.-C. Hladky-Hennion, J. L. Izbicki, P. Pareige, and M. Bruneau, *J. Appl. Phys.* **104**, 074909 (2008).
- <sup>26</sup>D. Royer and E. Dieulesaint, *Elastic Waves in Solids I* (Springer, New York, 2000).
- <sup>27</sup>J. C. Lagarias, J. A. Reeds, M. H. Wright, and P. E. Wright, *SIAM J. Optim.* **9**, 112 (1998).
- <sup>28</sup>R. Fiorito, W. Madigosky, and H. Uberall, *J. Acoust. Soc. Am.* **66**, 1857 (1979).